Materials Science and Engineering C 46 (2015) 538–547

Contents lists available at ScienceDirect

Materials Science and Engineering C

journal homepage: www.elsevier.com/locate/msec

# Fine tuning of magnetite nanoparticle size distribution using dissymmetric potential pulses in the presence of biocompatible surfactants and the electrochemical characterization of the nanoparticles

A. Rodríguez-López [a], J.J. Cruz-Rivera [b], C.G. Elías-Alfaro [b], I. Betancourt [c], H. Ruiz-Silva [d], R. Antaño-López [d,*]

[a] Centro Nacional de Metrología, Km 4.5 Carretera a Los Cués, C. P. 76246 El Marqués, Querétaro, Mexico
[b] Instituto de Metalurgia, Facultad de Ingeniería, Universidad Autónoma de San Luis Potosí, Sierra Leona No. 550, Lomas segunda sección, C. P. 78210 San Luis Potosí, SLP, Mexico
[c] Departamento de Materiales Metálicos y Cerámicos, Instituto de Investigaciones en Materiales, Universidad Nacional Autónoma de México, México, D. F. C.P. 04510, Mexico
[d] Centro de Investigación y Desarrollo Tecnológico en Electroquímica, S. C. Parque Tecnológico Querétaro — Sanfandila, C.P. 76703 Pedro Escobedo, Querétaro, Mexico

ARTICLE INFO

*Article history:*
Received 30 June 2014
Received in revised form 13 September 2014
Accepted 21 October 2014
Available online 23 October 2014

*Keywords:*
Electrochemical synthesis
Dissymmetric pulses
Magnetite nanoparticles
Biocompatible surfactants

ABSTRACT

The effects of varying the surfactant concentration and the anodic pulse potential on the properties and electrochemical behaviors of magnetite nanoparticles were investigated. The nanoparticles were synthesized with an electrochemical method based on applying dissymmetric potential pulses, which offers the advantage that can be used to tune the particle size distribution very precisely in the range of 10 to 50 nm. Under the conditions studied, the surfactant concentration directly affects the size distribution, with higher concentrations producing narrower distributions. Linear voltammetry was used to characterize the electrochemical behavior of the synthesized nanoparticles in both the anodic and cathodic regions, which are attributed to the oxidation of $Fe^{2+}$ and the reduction of $Fe^{3+}$; these species are part of the spinel structure of magnetite. Electrochemical impedance spectroscopy data indicated that the reduction and oxidation reactions of the nanoparticles are not controlled by the mass transport step, but by the charge transfer step. The sample with the highest saturation magnetization was that synthesized in the presence of polyethylene glycol.



## 1. Introduction

Magnetite ($Fe_3O_4$) is a material with diverse applications: in the environmental field it is widely used in the separation of metals from wastewater, and in industry it is extensively used in magnetic ink [1]. In recent years, magnetite has also been used in biomedical applications such as cell targeting, cell separation, drug delivery, and hyperthermia treatment [2–6].

Several methods have been described for synthesizing magnetite nanoparticles: for the chemical co-precipitation and microemulsion approaches, poor control of the particle size and the particle size distribution are unsolved problems [7,8], but the tight control of particle size and the particle size distribution is essential for some applications [7,9]. The addition of a surfactant in these methods addresses this problem to a certain extent, but the precise potential regulation that is possible in electrochemical methods enables the fine control of the magnetite particle size and particle size distribution [7,9–16].

It is common to coat magnetite nanoparticles with a surface active agent, such as ethylene glycol [7], to prevent agglomeration, and at the same time to protect the particles from oxidation by oxygen [13,17,18]. The surfactants that have been employed in the synthesis of magnetite nanoparticles include sodium oleate [14,19], polyethylene glycol [9,19,20], oleic acid [19,21,22], polyvinylpyrrolidone [23], and others [24]. For biomedical applications, the nanoparticles and their coatings must be biocompatible and have a suitable size and size distribution.

Previously, we proposed a new method for the synthesis of magnetite nanoparticles that uses dissymmetric potential pulses, and demonstrated that this method is useful in aqueous media [25]. In this method, the effects of mass transport during synthesis [3,8] are minimized by the selection of the pulse duration. We have previously established that the anodic potential and the duration of the pulse determine whether magnetite or maghemite is favored.

In this study, by using the novel method which offers indicated advantages [25], we assessed the effects of the presence of three different biocompatible surfactants at various concentrations in the synthesis of magnetite nanoparticles on their electrochemical behaviors and properties.

## 2. Experimental

### 2.1. Electrochemical system

A three-electrode glass cell with a capacity of 50 mL was employed. Pieces of high purity iron (Goodfellow, 99.5%) with a geometric area of

* Corresponding author.
*E-mail address:* rantano@cideteq.mx (R. Antaño-López).

http://dx.doi.org/10.1016/j.msec.2014.10.052
0928-4931/

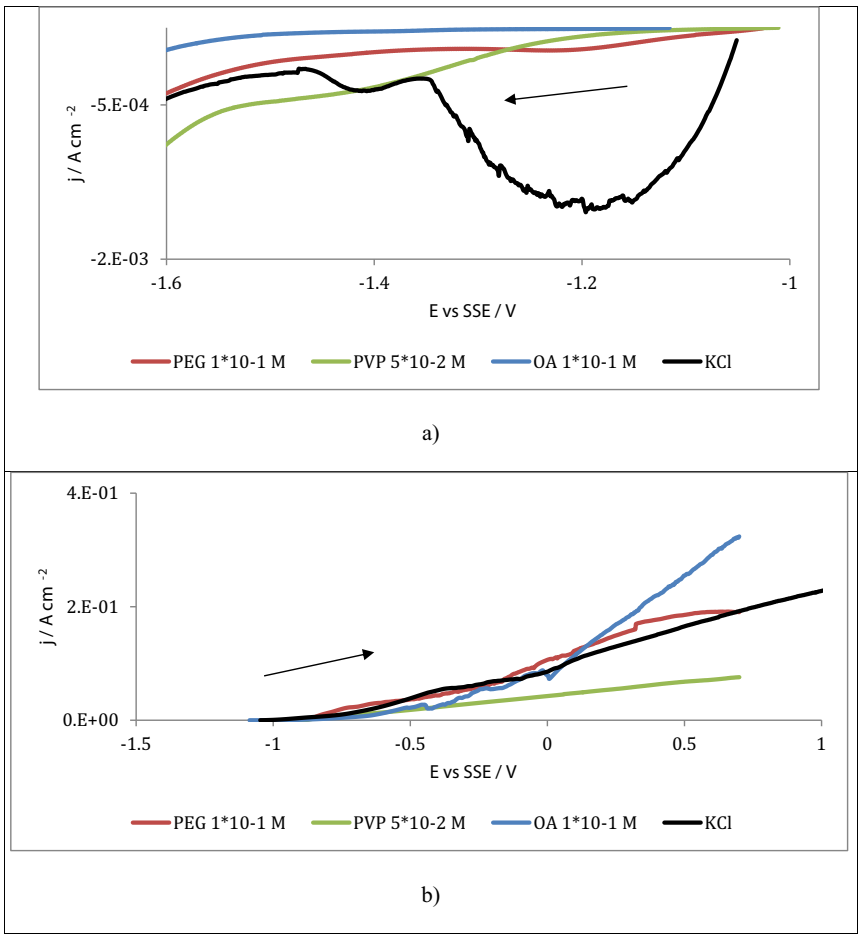


**Fig. 1.** Linear voltammetry in the cathodic (a) and anodic (b) directions, obtained in KCl 0.5 M and in the presence of three different surfactants. Scan speed 2 mV $s^{-1}$.

4 $cm^2$ were used as the working and counter electrodes. The reference electrode was a mercury–mercurous sulfate saturated electrode (SSE). The distance between the working and counter electrodes was set at 3 cm.

Polyethylene glycol (PEG, molecular weight 1000), polyvinylpyrrolidone (PVP molecular weight 10,000), and oleic acid (OA) were dissolved at three different concentrations in KCl 0.5 M. The solutions were prepared with ACS grade reagents and deionized water. The experiments were performed at environmental temperature and atmospheric pressure.

### 2.2. Syntheses

Before each synthesis, the system was stabilized for 3 to 5 min. The criterion for stabilization was 10 mV per minute as the maximum derivative. The solution was maintained without stirring. Slow linear voltammetry (2 mV/s) was carried out in order to identify and select the reduction and oxidation potentials of the iron ions and to evaluate the electrochemical stability of the medium. In order to select the duration of the potential pulses, chronoamperometric measurements were performed. We applied the design of experiments (DOE) method with

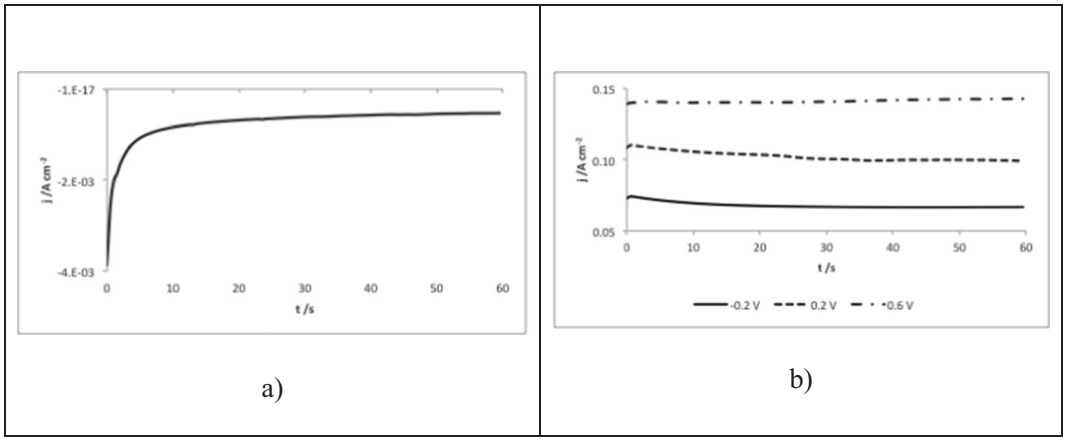


**Fig. 2.** Current behaviors at various pulse potentials: a) cathodic at −1.5 V vs SSE, and b) anodic potentials vs SSE.

the software JMP4 (SAS Institute Co.) to this information to elaborate an experimental model. A $2^n$ model was created, with $n = 3$: surfactant type, surfactant concentration, and anodic potential. One repetition for experiment was considered, and an experimental design with 38 tests was obtained. In additional experiments, two further samples were synthesized in the absence of surfactant. The syntheses were carried out by using a potentiostat/galvanostat PARSTAT 2273 (Princeton Applied Research).

### 2.3. Characterization of the powders

The suspended particles were washed three times with water and a final wash was performed with ethanol by using a centrifuge (Hermle, model Z206A) at 5000 rpm for 15 min to separate the solid from the liquid in each wash. The product was then lyophilized (Labconco, Freezone 2.5) for 60 min at −50 °C. The powders were characterized with XRD, TEM, and VSM.

The XRD experiments were performed immediately after the powders were obtained in order to minimize the oxidation of the powders by oxygen in the air. Diffractograms were collected for 2θ values from 20° to 90° by using a Bruker D8 Advance with $CuK_\alpha$ radiation. The crystal size of each sample was estimated from the broadening of the (3 1 1) plane signal in its diffractogram by using the Scherrer equation:

$$d = \frac{0.89 \cdot \lambda}{\beta \cdot \cos\theta}$$

where d is the mean length of the crystal, λ is the wavelength of the radiation, β is the line broadening, and θ is the diffraction angle.

**Table 1**
Design of experiments.

| Sample | Surfactant | Concentration/M | Anodic potential/V vs SSE |
|---|---|---|---|
| 1 | PEG | 1 E−3 | 0.6 |
| 2 | OLEIC ACID | 1 E−5 | −0.2 |
| 3 | PEG | 1 E−1 | 0.6 |
| 4 | PVP | 1 E−5 | 0.6 |
| 5 | PEG | 1 E−1 | 0.2 |
| 6 | PEG | 1 E−1 | 0.6 |
| 7 | PEG | 1 E−1 | −0.2 |
| 8 | PEG | 1 E−5 | 0.6 |
| 9 | OLEIC ACID | 1 E−3 | 0.6 |
| 10 | PVP | 1 E−5 | 0.6 |
| 11 | PVP | 1 E−5 | −0.2 |
| 12 | PVP | 5 E−2 | 0.6 |
| 13 | PVP | 1 E−3 | 0.6 |
| 14 | OLEIC ACID | 1 E−5 | −0.2 |
| 15 | PVP | 1 E−3 | −0.2 |
| 16 | PEG | 1 E−5 | 0.6 |
| 17 | OLEIC ACID | 1 E−1 | −0.2 |
| 18 | PEG | 1 E−5 | −0.2 |
| 19 | OLEIC ACID | 1 E−1 | 0.6 |
| 20 | PEG | 1 E−3 | −0.2 |
| 21 | PEG | 1 E−3 | −0.2 |
| 22 | PEG | 1 E−1 | −0.2 |
| 23 | PVP | 1 E−3 | −0.2 |
| 24 | OLEIC ACID | 1 E−1 | −0.2 |
| 25 | PEG | 1 E−5 | −0.2 |
| 26 | OLEIC ACID | 1 E−5 | 0.6 |
| 27 | PEG | 1 E−1 | 0.2 |
| 28 | OLEIC ACID | 1 E−3 | −0.2 |
| 29 | OLEIC ACID | 1 E−1 | 0.6 |
| 30 | OLEIC ACID | 1 E−3 | 0.6 |
| 31 | PEG | 1 E−3 | 0.6 |
| 32 | OLEIC ACID | 1 E−3 | −0.2 |
| 33 | PVP | 1 E−5 | −0.2 |
| 34 | OLEIC ACID | 1 E−5 | 0.6 |
| 35 | PVP | 5 E−2 | 0.6 |
| 36 | PVP | 1 E−3 | 0.6 |
| 37 | PVP | 5 E−2 | −0.2 |
| 38 | PVP | 5 E−2 | −0.2 |

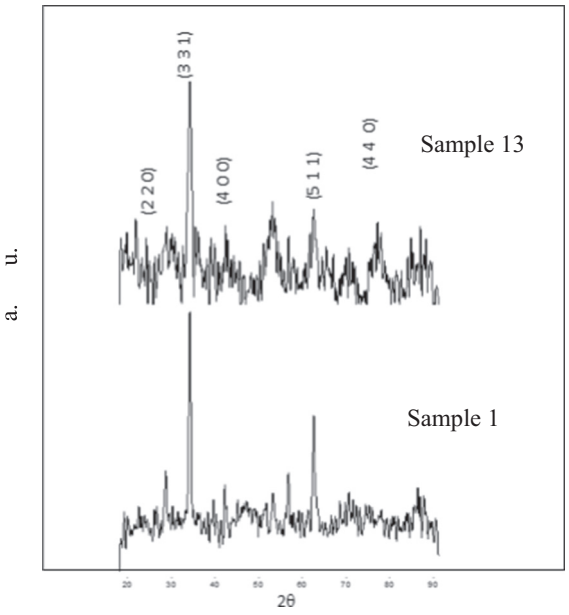


**Fig. 3.** Diffractograms obtained for samples synthesized in the presence of PEG and PVP (samples 1 and 13 in Table 1).

TEM (JEM 1230 JEOL) measurements were carried out to analyze the size and shape of the particles. Suspensions of the powders in ethanol were prepared in an ultrasound bath for 10 min, then one drop of each suspension was placed onto a carbon-coated copper grid and the solvent was allowed to evaporate. The average particle size and the size distribution of each prepared sample were estimated by measuring the diameters of at least 120 particles by means of image treatment.

To determine the hysteresis curves and hence the saturation magnetization ($M_s$) of the nanoparticle samples, vibrating sample magnetometry (VSM) experiments were carried out at room temperature by using a LDJ model 9600 magnetometer with a maximum applied field of 15 kOe.

To determine the electrochemical behaviors of the magnetite nanoparticle samples synthesized in the presence and absence of surfactants, linear voltammetry (LV) and electrochemical impedance spectroscopy (EIS) were performed. Three carbon paste electrodes were prepared: a blank electrode without magnetite, an electrode with magnetite synthesized in the absence of surfactant, and an electrode with magnetite synthesized in the presence of surfactant.

The LV experiments were performed under open circuit potential (OCP) conditions for both the cathodic and anodic domains. EIS experiments were carried out at various potentials, including OCP, in the

**Table 2**
Crystal sizes estimated from main broadening with the Scherrer equation.

| Sample number | Size/nm | Sample number | Size/nm |
|---|---|---|---|
| 1 | 17.9 | 15 | 18.6 |
| 2 | 24.3 | 17 | 19.0 |
| 3 | 18.2 | 18 | 23.0 |
| 4 | 17.5 | 19 | ND |
| 5 | 17.9 | 20 | 26.5 |
| 7 | 21.4 | 26 | 16.8 |
| 8 | 21.3 | 28 | 20.8 |
| 9 | 19.0 | 37 | 15.1 |
| 11 | 20.4 | FD+ | 17.9 |
| 12 | 14.4 | FD++ | 22.4 |
| 13 | 23.0 | | |

ND: Not determined.
OD+: Additional experiment, out of design of experiment, no surfactant, −0.2 V vs SSE as anodic pulse. OD++: Additional experiment, out of design of experiments, no surfactant, 0.6 V vs SSE as anodic pulse.

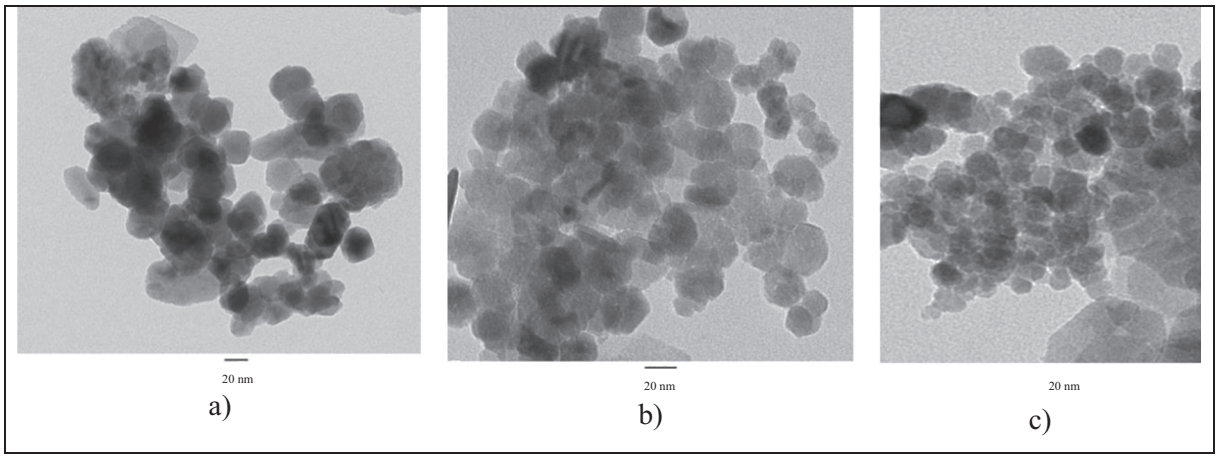


**Fig. 4.** TEM images of samples synthesized in the presence of surfactants: a) PEG, b) PVP, and c) oleic acid (samples 1, 13, and 9 in Table 1 respectively).

frequency range 10 kHz to 10 mHz, 7 points per decade, by using a potentiostat/galvanostat PARSTAT 2273. The electrolyte used in these experiments was HCl (reagent grade) 1 M, deoxygenated for 15 min with a $N_2$ purge before each experiment.

## 3. Results and discussion

### 3.1. Electrochemical syntheses

Fig. 1 shows the typical voltammetric behaviors of potential scans in the cathodic and anodic directions. Two reduction signals can be seen in the cathodic direction, the first at −1.2 V vs SSE and the second at −1.4 V vs SSE. In the anodic direction, there are no oxidation peaks, but there is a marked change in the slope at −0.3 V vs SSE. These results are in agreement with those of a previous report [25], in which the first cathodic peak was attributed to the reduction of ferric ions to ferrous ions and the second cathodic peak was assigned to the reduction of ferrous ions to metallic iron; however, proton reduction cannot be excluded because of the absence of evidence of metallic iron. The change in the slope of the anodic scan corresponds to a change in the oxidation process, such as perhaps ferrous to ferric oxidation or water hydrolysis. Considering the results in Fig. 1, and those of a previous study [25], we decided to keep the cathodic pulse constant at −1.5 V vs SSE for all of the experiments, but selected two potentials, −0.2 V and 0.6 V vs SSE, for the anodic pulses.

To determine the appropriate durations of the pulses, transient current curves were built for the selected potential pulses. These results are shown in Fig. 2. Note that when the cathodic potential is applied (2a) a small current is observed ($10^{-3}$ A/cm$^2$), because at the beginning there are no Fe(II) or Fe(III) electroactive species to reduce. This current tends toward zero: it is almost constant after 8 or 10 s. Thus, in order to prevent diffusion-controlled processes, 5 s was selected as the cathodic pulse duration. When the anodic potential is applied to the system, the current increases with the potential, as expected, which indicates that Fe(II) and Fe(III) ions are electrogenerated. In addition, note that current stabilization is faster when the potential is increased, so a stabilization time of 10 s was selected because it is the stabilization time for the highest potential pulse (0.6 V vs SSE). With this approach, we can be certain that the whole process is not limited by mass transport under the selected conditions. Based on these results, we established the conditions for the experiments, as shown in Table 1.

In addition, two more syntheses without surfactant were performed in the electrolytic media at both anodic potentials. In both cases, the solution changed from colorless to black after a few minutes. This qualitative result indicates that the formation of the magnetite phase is favored over those of other phases. At the highest concentration of both oleic acid and PVP, the nanoparticles are strongly embedded in the surfactant, forming a film, thus no powders were obtained. These experiments were then excluded from discussion.

**Table 3**
Average sizes and standard deviations obtained from TEM images.

| Consecutive design of experiments | Size/nm | |
|---|---|---|
| | Average | Standard deviation |
| 1 | 22.5 | 9.1 |
| 3 | 27.8 | 7.4 |
| 4 | 22.4 | 8.1 |
| 8 | 31 | 11 |
| 9 | 20.5 | 8.1 |
| 13 | 20.0 | 7.3 |
| 15 | 26.6 | 6.6 |
| 20 | 22.7 | 9.7 |
| 26 | 21.8 | 6.2 |
| 28 | 20.4 | 6.1 |

### 3.2. Characterization of the powders

#### 3.2.1. X-ray diffraction (XRD)

Two representative XRD diffractograms of synthesized iron oxide nanoparticles are shown in Fig. 3. These diffractograms are for samples produced in the presence of PEG and PVP at a medium concentration and 0.6 V vs SSE (samples 1 and 13 in Table 1). The diffractograms were compared against those in the database for magnetite, maghemite, hematite, goethite, and metallic iron. As expected, no metallic iron was detected in any sample, which is in agreement with results obtained in the absence of surfactant [25]. The experimental diffractograms match

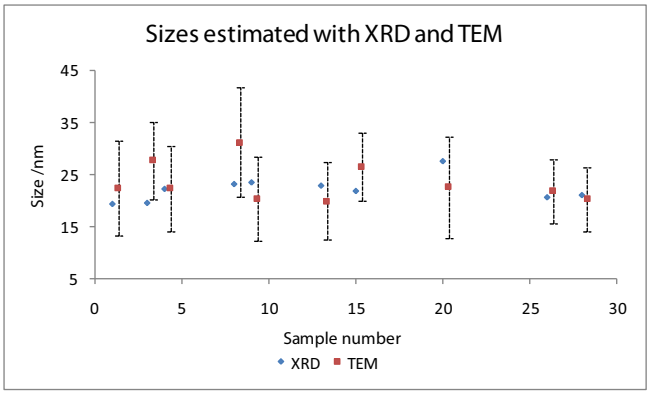


**Fig. 5.** Comparison of average sizes and standard deviations estimated with XRD and TEM.

those of magnetite and maghemite, but are especially good matches to that of magnetite. Further, the powders are black, so we can assume that magnetite is the main phase [1].

By using the Scherrer equation, the crystal size of each sample was estimated from the broadening of the (3 1 1) plane in its diffractogram, and the obtained values are presented in Table 2. The estimated values indicate that the particles are nanoscale in size. The average sizes are in the range of 14 to 27 nm, which is similar to that obtained without surfactant, for which the range was found to be 14 to 22 nm [25]. For sample 19, which was synthesized in the presence of oleic acid at the highest concentration, no well-defined pattern was obtained. Thus, our main initial finding is that the electrochemical method can be used to control the size range, regardless of the presence of the surfactant.

*3.2.2. Transmission electron microscopy (TEM)*

To confirm the results obtained with XRD, ten samples were analyzed with TEM in order to evaluate the effects of varying the surfactant and anodic potential on particle size. These samples correspond to sample numbers 1, 3, 4, 8, 9, 13, 15, 20, 26, and 28 in Table 1. Three images obtained from samples synthesized at medium concentrations of the surfactants and with an anodic pulse potential of 0.6 V vs SSE are shown in Fig. 4.

These results confirm that the nanoparticles are of nanometric sizes with quasi-spherical shapes. The average sizes and standard deviations, as determined with image treatment, are shown in Table 3. The average sizes are in the range of 20 to 31 nm, which is narrower than obtained without surfactants [25], for which the estimated sizes are in the range of 10 to 50 nm. This reduction in the size range indicates that there is less agglomeration when surfactants are present during the syntheses. The average sizes and standard deviations obtained with TEM and the sizes estimated with XRD are shown in Fig. 5. There are some differences between the sizes estimated with XRD and averages obtained with TEM. It has been reported that different methods can produce results that are somewhat different [26]. We attribute these differences to the differences between the particular principles of measurement of these techniques. However, in almost all these cases the XRD size estimate is within one standard deviation of the TEM size estimate. If twice the standard deviation of each TEM result is used, which corresponds to 95.4% of the distribution, all the XRD estimates are in good agreement with the TEM results.

Although narrower size distributions are synthesized in the presence of surfactants than in their absence, these differences are not extreme, which confirms that the size distribution depends mainly on the parameters of the electrochemical method.

To investigate further the effects of varying the surfactant and anodic potential on the size distributions of the nanoparticles, the data obtained with TEM were employed to construct a histogram of the results for every sample. The significant results are discussed below.

The effects of varying the PEG concentration during synthesis when an anodic pulse potential of 0.6 V vs SSE is applied are shown in Fig. 6. Note that the form of the size distribution depends on the surfactant concentration: the distribution becomes narrower and more Gaussian as the surfactant concentration is increased. The effects on the size distribution of varying the concentrations of the other surfactants at low and medium concentrations are presented in Fig. 7. In this figure, we can see that when the concentration is increased the size distribution exhibits kurtosis toward the lower sizes, which is expected because surfactants prevent agglomeration, and thus limit the growth of particles. Similar results were observed for the other surfactants.

The effects of varying the potential of the anodic pulse on the size distribution are shown in Fig. 8. According to Pascal and Cabrera [27,28], higher potentials result in reduced dispersion. However, in our results the size distribution is almost insensitive to changes in the anodic pulse potential up to 800 mV. But it is worthy to note that we can obtain similar results applying smaller potentials to make the process more efficient.

That information is an important contribution of this optimization study, where it is evident that some changes on the simple electrochemical method, can offer different characteristics of magnetite nanoparticles.

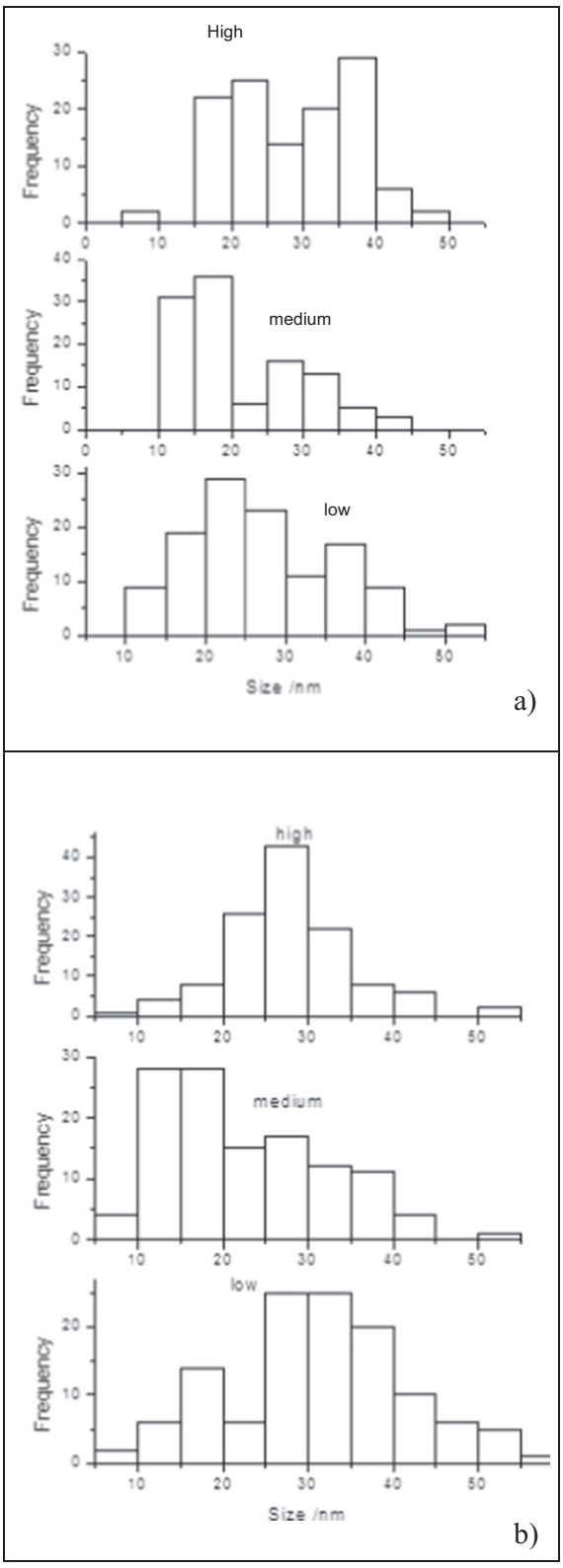


**Fig. 6.** Size distributions obtained with TEM for samples synthesized (a) in the absence of surfactants and (b) in the presence of PEG at three different concentrations, with an anodic pulse potential of 0.6 V vs SSE.

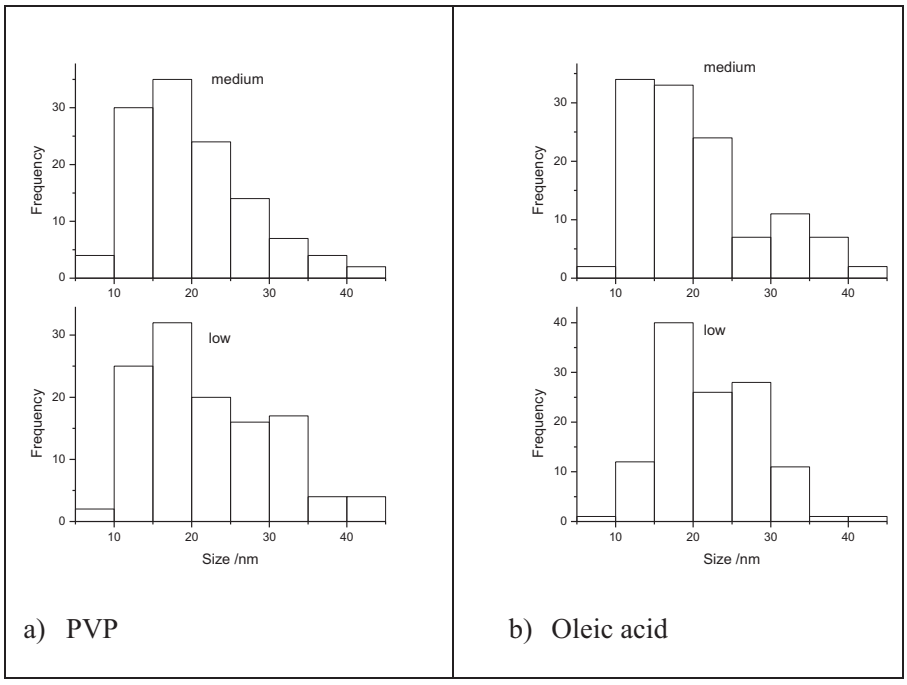


**Fig. 7.** Size distributions obtained with TEM for samples synthesized in the presence of PVP and oleic acid at two different concentrations, with an anodic pulse potential of 0.6 V vs SSE.

*3.2.3. Vibrating sample magnetometry (VMS)*

According to Cornell [1], micrometric magnetite has a saturation magnetization of 92–100 emu $g^{-1}$, with a value for maghemite of 60–80 emu $g^{-1}$, although smaller values for magnetite nanoparticles have been reported and attributed to nanoscale effects [29]. The hysteresis curves of several samples including material synthesized without surfactants are shown in Fig. 9. For all of the samples, saturation is reached below 5 kOe, which indicates the soft magnetic character of the nanoparticles. In the case of the nanoparticles synthesized with our method, the highest and medium concentration PEG samples have the highest magnetic saturation, 70.8 emu $g^{-1}$. Although it is necessary to perform more fundamental studies; that behavior is probably due to the fact that functional groups of PEG have stronger interactions with the magnetite nanoparticle than the other surfactants, thus it protects more effectively the magnetite against oxidation, which lowers magnetic saturation.

*3.2.4. Linear voltammetry (LV)*

Fig. 10 shows the cathodic and anodic linear voltammetry results. The blank makes a negligible contribution to the response of the electrodes containing the synthesized mineral. The current densities of the magnetite nanoparticles synthesized in the presence of surfactant or in its absence and supported on carbon paste electrodes are of the same order of magnitude.

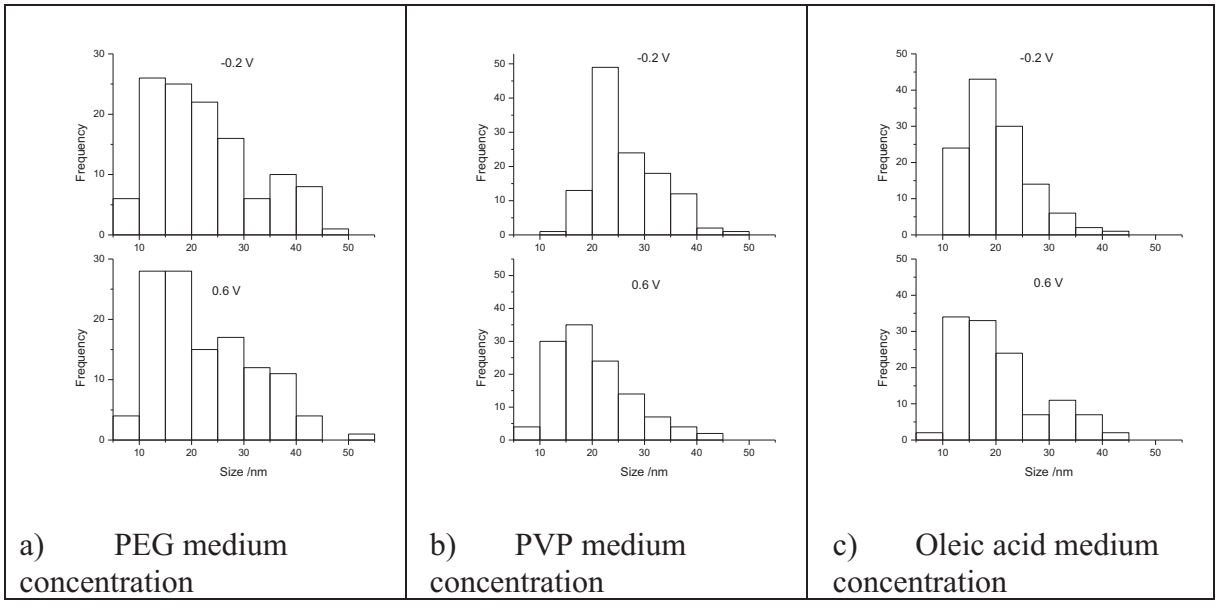


**Fig. 8.** Effects of varying the anodic pulse potential on the size distributions (obtained with TEM) for three different surfactants at medium concentration.

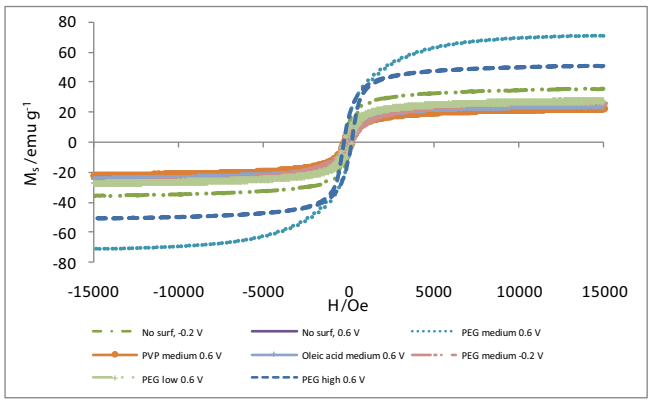


**Fig. 9.** Hysteresis curves for synthesized nanoparticles.

The cathodic scans in Fig. 10a feature a wide peak under both conditions, which indicates that the reduction process comprises different energetic stages. This fact is probably related to the availability of Fe(II) and Fe(III) ions on the surfaces of the nanoparticles, which have spinel structure. It is remarkable that the reduction behaviors under both sets of conditions are very similar, although the open circuit potential moves to a more cathodic value when the magnetite nanoparticles were synthesized in the presence of surfactants, which means that the electrochemical interface has changed.

In the anodic scans in Fig. 10b, the oxidation peak attributed to ferrous species oxidation [30,31] moves toward more anodic potentials, which indicates that the magnetite nanoparticles are coated with more surfactant and thus it is more difficult for the ions in the crystal lattice to react. Note also that the peak is broad, as in the cathodic scan, and can be explained in similar terms.

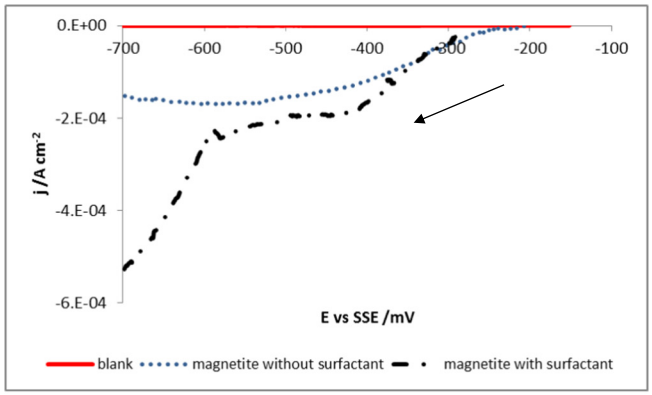


a)

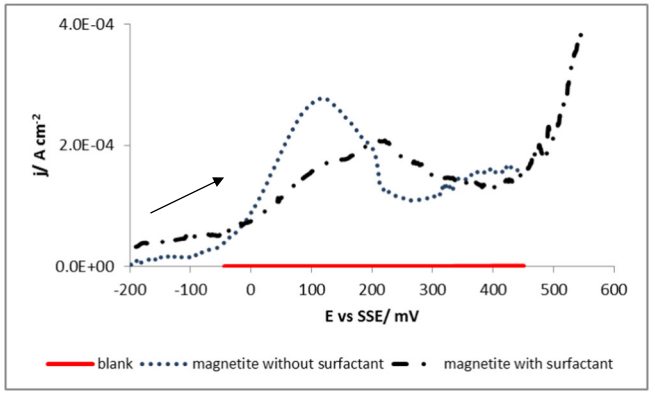


b)

**Fig. 10.** Cathodic (a) and anodic (b) linear sweep voltammograms for three electrodes in 1 M HCl at 2 mV/s.

*3.2.5. Electrochemical impedance spectroscopy (EIS)*

EIS was performed to determine the electrochemical stabilities of the magnetite nanoparticles. First, we analyzed the possible contributions of the carbon paste electrode. Fig. 11 shows the Nyquist and Bode phase diagrams obtained for a blank sample. In the Nyquist diagram, a capacitive contribution is evident in almost all the studied frequency intervals; this behavior is confirmed in the Bode phase diagram, where capacitive behavior is predominant for almost all the frequencies tested.

Fig. 12 shows the Nyquist diagrams of electrodes containing magnetite synthesized in the presence of surfactant and in its absence. For both the cathodic and anodic cases, one semicircle is relatively well defined at high frequencies and another, not well defined, appears at low frequencies. The semicircle at high frequencies is associated with the electrochemical reactions of magnetite, which comprise the reduction of Fe(III) at cathodic potentials and the oxidation of Fe(II) at anodic potentials, in the spinel structure. The second semicircle at low frequencies is attributed to the adsorption of intermediate species, as usually assumed in mechanistic impedance studies [29] even if the identities of these intermediate species cannot be determined.

Fig. 12a and b shows that in the absence of the surfactant, the main changes in the spectra concern the low frequency loop, which is usually attributed to adsorption phenomena. In the case of the cathodic domain, Fig. 12a, the loop size decreases as the cathodic potential becomes more negative: It means that intermediates adsorption process enhances the overall reduction reaction. On the contrary, the anodic behavior, Fig. 12b, shows that this loop grows as the potential become more anodic. In this case the intermediate adsorption phenomena hinder at some degree the magnetite's oxidation reaction.

In contrast, in the presence of the surfactant, Fig. 12c and d, the spectra changes with potential are less notorious. This is attributed to the adsorption of the surfactant, which predominates over the adsorption of any other species. It implies that the size of the low frequency loop remains insensitive to changes in the polarization potential, except for the more cathodic potential. In this case, significant changes are observed at high frequency loop, which means that a new reduction process is favored at this potential. Deeper studies are necessary to unveil the nature of this process.

The impedance spectra were fitted by using the program Z-View with the Levenberg–Marquardt algorithm and the equivalent circuit shown in Fig. 12e, which have been used to fit such spectra in earlier studies [22]. In this circuit, the electrolyte resistance (R1) is in series with the charge transfer resistance (Rct) (R2) and in parallel with the constant phase element (CPE1), which in this case represents the non-ideal double layer capacitance (Cdl); in addition, a final R3–CPE3 coupled in parallel is associated with the adsorption process.

In this fit, we are mainly interested in R2, which is associated with the charge transfer resistance that corresponds to the stability of the nanoparticles. The dependence of this resistance on the polarization potential is shown in Fig. 13 for both cathodic and anodic polarizations, in the presence of surfactant and in its absence. As can be seen in this figure, the resistance is on average larger when the nanoparticles are synthesized in the presence of surfactants. This result indicates that the nanoparticles are coated with surfactant, and that they are more stable. Nonetheless, Rtc data indicate that this stability enhancement is not dramatic.

## 4. Conclusions

Magnetite nanoparticles were successfully synthesized by applying dissymmetric potential pulses in the presence of biocompatible surfactants; this approach was found to produce quasi-spherical nanoparticles with sizes in the range of 10 to 50 nm.

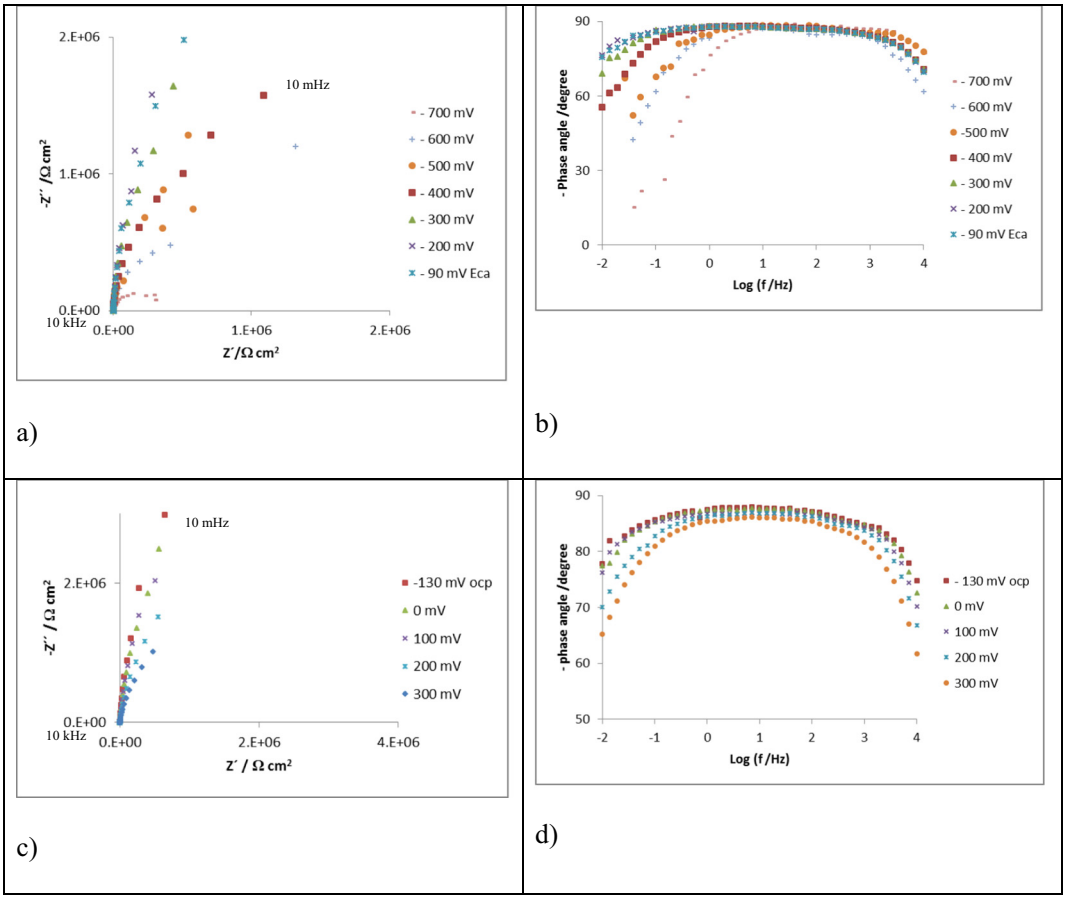


**Fig. 11.** Impedance spectra obtained for the blank in 1 M HCl at various cathodic (a, b) and anodic (c, d) overpotentials. Nyquist (a, c) and Bode phase (b, d) diagrams.

Although varying the surfactant concentration does not affect the average size of the nanoparticles, it does alter their size distribution: narrower distributions arise at higher surfactant concentrations. For the variation in the anodic pulse potentials that we studied, there are no effects on the average size or the size distribution, so it is possible to produce magnetite nanoparticles with similar characteristics by using less energy, which makes the process more efficient and interesting because it is possible to control size distribution changing relatively simple variables.

Our results for the saturation magnetization of the nanoparticles indicate that the best electrochemical synthesis condition is the use of PEG at high concentrations, because under these conditions the highest saturation value is observed.

Our LV and EIS results confirm that the magnetite nanoparticles are coated with surfactant; the changes in the open circuit potential and the overpotential needed for reduction or oxidation grow with increases in the surfactant concentration. Moreover, the charge transfer resistance increases when the nanoparticles are synthesized in the presence of surfactant.

## Acknowledgments

The authors thank CONACYT and CONCYTEG, México, for their financial support of this study through project GTO-2008-C03-91691.

The authors also thank Dr. J. J. Pérez Bueno, Dr. L. A. Ortiz Frade, and Dr. F. Rodríguez Valadez for their assistance in this study.

Rodríguez-López A. also acknowledges CONACYT and CENAM (96461), México, for their support of his Ph. D. studies.

## References

[1] R.M. Cornell, U. Schwertmann, The Iron Oxides. Structure, Properties, Reactions, Occurrences and Uses, 2 ed. Wiley-VCH, Weinheim, 2003.
[2] C. Tsouris, et al., Electrocoagulation for magnetic seeding of colloidal particles, Colloids Surf. A Physicochem. Eng. Aspects 177 (2001) 11.
[3] T.-Y. Ying, S. Yiacoumi, C. Tsouris, An electrochemical method for the formation of magnetite nanoparticles, J. Dispers. Sci. Technol. 23 (4) (2002) 8.
[4] R.F.C. Marques, et al., Electro-precipitation of $Fe_3O_4$ nanoparticles in ethanol, J. Magn. Magn. Mater. 320 (2008) 5.
[5] Z. Li, et al., Magnetite nanoparticles with high heating efficiencies for application in the hyperthermia of cancer, Mater. Sci. Eng. C 30 (7) (2010) 990–996.
[6] G. Zhang, Y. Liao, I. Baker, Surface engineering of core/shell iron/iron oxide nanoparticles from microemulsions for hyperthermia, Mater. Sci. Eng. C 30 (1) (2010) 92–97.
[7] P. Tartaj, et al., The preparation of magnetic nanoparticles for applications in biomedicine, J. Phys. D. Appl. Phys. 36 (2003) 16.
[8] S. Franger, P. Berthet, J. Berthon, Electrochemical synthesis of $Fe_3O_4$ nanoparticles in alkaline aqueous solutions containing complexing agents, J. Solid State Electrochem. 8 (2004) 6.
[9] T. Theppaleak, et al., Synthesis of water dispersible magnetite nanoparticles in the presence of hydrophilic polymers, Polym. Bull. 63 (2009) 12.
[10] W. Tan, S. Santra, P. Zhang, R. Tapec, J. Dobson, Coated Nanparticles, US6548264 B1, University of Florida, 2003.
[11] V.G. Belikov, A.G. Kuregyan, Synthesis of magnetite complexes with drugs, Pharm. Chem. J. 38 (3) (2004) 4.
[12] G. Marinescu, et al., Synthesis of magnetite nanoparticles in the presence of aminoacids, J. Nanoparticle Res. 8 (2006) 7.
[13] A.-H. Lu, E.L. Salabas, F. Schuth, Magnetic nanoparticles: synthesis, protection, functionalization, and application, Angew. Chem. 46 (2007) 23.
[14] H. Yue-hua, et al., Dispersion mechanism of nano-magnetite coated with oleate in aqueous carrier, J. Cent. South Univ. Technol. 15 (2008) 6.
[15] F. Zhang, et al., Synthesis and characterization of polystyrene-grafted magnetite nanoparticles, Colloid Polym. Sci. 286 (2008) 5.
[16] A.S. Teja, P.-Y. Koh, Synthesis, properties, and applications of magnetic iron oxide nanoparticles, Prog. Cryst. Growth Charact. Mater. 55 (2009) 24.
[17] T. Osaka, et al., New trends in nanoparticles: syntheses and their applications to fuel cells, health care, and magnetic storage, Isr. J. Chem. 48 (2008) 15.

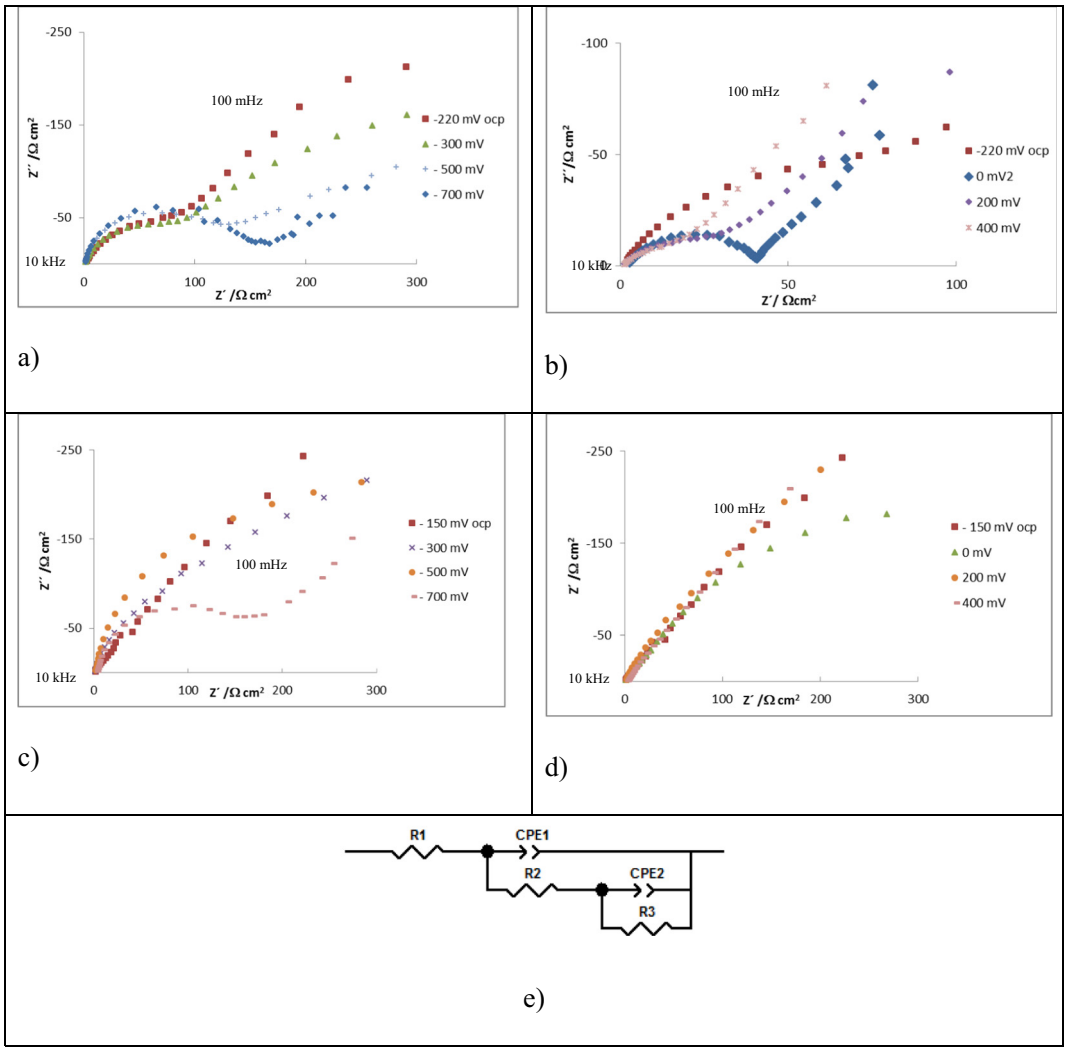


**Fig. 12.** Impedance spectra obtained for magnetite electrodes without (a, b) and with (c, d) surfactant in 1 M HCl at various cathodic (a, c) and anodic (b, d) overpotentials. e) Equivalent circuit used for fitting.

[18] M.E. Khosroshahi, L. Ghazanfari, Synthesis and functionalization of $SiO_2$ coated $Fe_3O_4$ nanoparticles with amine groups based on self-assembly, Mater. Sci. Eng. C 32 (5) (2012) 1043–1049.
[19] Q. Wang, H. Yang, Morphology and magnetic properties of $Fe_xCo_{1-x}/Co_yFe_{3-y}O_4$ nanocomposites prepared by surfactants-assisted-hydrothermal process, J. Nanopart. Res. 11 (2009) 9.
[20] A. Skumiel, A. Jozefczak, T. Hornowski, Investigation of magnetic and hyperthermic effects in ferrofluids with PEG biocompatible surfactant, 11th Conference on Electrorheological Fluids and Magnetorheological Suspensions, IOP Publishing Ltd., 2009, p. 4.
[21] L.A. García-Cerda, et al., Síntesis y propiedades de ferrofluidos de magnetita, Superficies Vacío 16 (1) (2003) 4.
[22] X. Liu, et al., Preparation and characterization of hydrophobic superparamagnetic magnetite gel, J. Magn. Magn. Mater. (306) (2006) 6.
[23] H.L. Liu, et al., One-pot polyol synthesis of monosize PVP-coated sub-5 nm $Fe_3O_4$ nanoparticles for biomedical applications, J. Magn. Magn. Mater. 310 (2007) 3.
[24] F.J. Santos, et al., Synthesis and electrochemical behavior of single-crystal magnetite nanoparticles, J. Phys. Chem. 112 (2008) 6.
[25] A. Rodríguez-López, et al., Electrochemical synthesis of magnetite and maghemite nanoparticles using dissymmetric potential pulses, J. Nanoparticle Res. 14 (993) (2012) 9.
[26] R.C. Woodwart, et al., A comparison of methods for the measurement of the particle-size distribution of magnetic nanoparticles, J. Appl. Crystallogr. 40 (2007) 6.
[27] C. Pascal, et al., Electrochemical synthesis for the control of γ-$Fe_2O_3$ Nanoparticle size. Morphology, microstructure, and magnetic behavior, Chem. Mater. 11 (1) (1999) 7.
[28] L. Cabrera, et al., Magnetite nanoparticles: electrochemical synthesis and characterization, Electrochim. Acta 53 (2008) 6.
[29] S. Franger, et al., Large influence of the synthesis conditions on the physico-chemical properties of nanostructured $Fe_3O_4$, J. Nanoparticle Res. 9 (2007) 14.
[30] P. Encinas, et al., Electrochemical study of iron (II) and iron (III) compound mixtures in the solid state. application to magnetite characterization, J. Electroanal. Chem. 371 (1994) 6.
[31] P. Periasamy, B.R. Babu, S.V. Iyer, Cyclic voltammetric studies of porous iron electrodes in alkaline solutions used for alkaline batteries, J. Power Sources 58 (1996) 6.

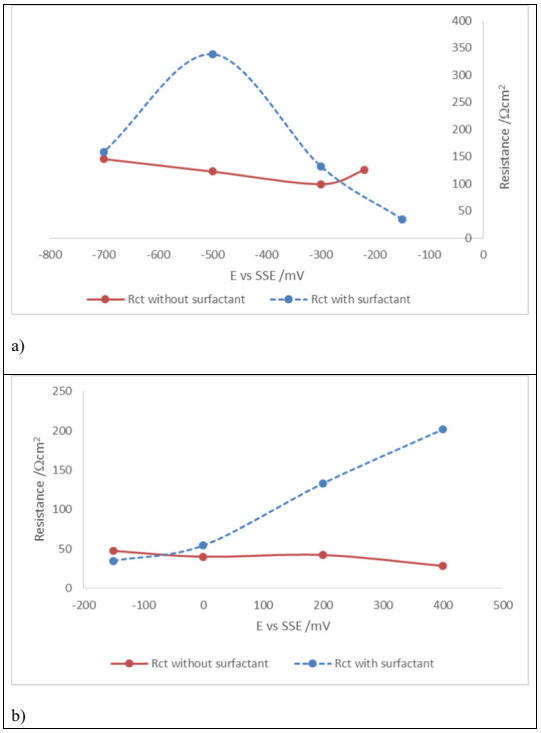


**Fig. 13.** Dependence of the charge transfer resistances on the cathodic (a) and anodic (b) overpotentials. Carbon paste electrodes with magnetite synthesized in the presence of surfactant and in its absence, 1 M HCl.